Assessing the suitability of three proxy sources for the development of detectors of special nuclear materials

Journal of Radiological Protection

Official journal of the Society for Radiological Protection

PAPER • **OPEN ACCESS**

Assessing the suitability of three proxy sources for the development of detectors of special nuclear materials

To cite this article: Matthew P Taggart *et al* 2020 *J. Radiol. Prot.* **40** 1138

OPEN ACCESS
IOP Publishing | Society for Radiological Protection
Journal of Radiological Protection
J. Radiol. Prot. **40** (2020) 1138–1153 (16pp)
https://doi.org/10.1088/1361-6498/ab9fdb

Assessing the suitability of three proxy sources for the development of detectors of special nuclear materials

Matthew P Taggart[1,4], Chris Allwork[2], Michael Collett[2], Michael W J Hubbard[1] and Paul J Sellin[1]

[1] Department of Physics, University of Surrey, Guildford, Surrey, United Kingdom
[2] AWE PLC, Aldermaston, Berkshire, United Kingdom[3]

E-mail: m.taggart@surrey.ac.uk

Received 16 March 2020, revised 4 June 2020
Accepted for publication 24 June 2020
Published 22 September 2020

Abstract

Numerous techniques and equipment have been developed to provide a capability for the detection of special nuclear materials (SNM), but due to the necessary security measures surrounding these materials alternate, or proxy, neutron sources are often utilised in their stead. In this paper we report the neutron and gamma pulse shape discrimination response of plastic scintillator to mixed neutron/gamma beams produced from two radionuclide neutron sources, and also from an SNM source of weapons-grade plutonium. We discuss the suitability of using radionuclide sources, with appropriate shielding configurations as proxy sources for SNM.

A $3\sigma n_{th\text{-}\gamma}$ discrimination level has been achieved for an SNM source at a low-level energy threshold of ~220 keVee when a shielding configuration of 5 cm of lead was implemented. Varying amounts of lead and high-density polyethylene (HDPE) shielding were also investigated with the 3σ limit being reached by ~240 keVee.

This work shows that an AmBe neutron source serves as an appropriate SNM proxy achieving a comparable value for figure of merit above ~1 MeVee. For energies below 1 MeVee down to ~100 keVee a closer approximation of the expected FoM for SNM can be attained when using ^{252}Cf as a proxy source

[3] UK Ministry of Defence © Crown Owned Copyright 2019/AWE.
[4] Author to whom any correspondence should be addressed.

1361-6498/20/+16$33.00 Printed in the UK

or by utilising an 'enhanced' AmBe source with the addition of a further low energy γ ray source.

Keywords: neutron detection, pulse shape discrimination, silicon photomultiplier

(Some figures may appear in colour only in the online journal)

1. Introduction

The use of neutron discriminating plastic scintillators, such as the material produced by Eljen (most recently as EJ-276) [1, 2], coupled with a silicon photomultiplier (SiPM) readout has become increasingly commonplace in detection of special nuclear materials (SNM).

In this work we study the neutron/gamma pulse shape discrimination (PSD) properties of a plastic scintillator-SiPM system [7, 8] to assess the suitability of various radionuclide neutron sources as proxy sources for SNM. Various groups have previously reported the performance of PSD plastic scintillator using isotopic neutron sources of the (α,n) reaction type, such as AmBe [9–11], AmLi [12], ^{238}PuBe [13], and ^{238}PuC [14]. However, the energy spectra of both neutrons and gammas emitted from such sources are quite distinct from those of special nuclear materials (SNM) [3–5], which can lead to an overestimation of neutron-gamma separation performance when used in isolation. In order to assess a system's ability to identify SNM, it is often useful to use 'proxy' sources where a sample of SNM may not otherwise be available, namely ^{252}Cf [15–17], or one of the previously mentioned (α,n) sources. However, in these cases one must carefully consider the respective differences between the sources, namely, the energies of emission, and the multiplicities of those emitted particles. Similarly, it should not be overlooked that detector volume can play a role beyond simple detection efficiency with attenuation and timing becoming important factors for large-scale systems. Here we report a comparative study of the performance of a PSD plastic scintillator using two different radionuclide neutron sources ^{241}AmBe and ^{252}Cf plus a sample of weapons-grade plutonium ($<$7% ^{240}Pu [18, 19]) that will be referred to as the SNM source.

The neutron energy spectrum resulting from nuclear fission [20–22] follows a smooth Watt or Maxwellian distribution, whereas (α,n) sources, such as the AmBe used in this work, typically have greater structure in their neutron spectra [23, 24]. The spectra reproduced in figure 1 show the different energy spectra from of these common neutron sources. The AmBe source has a higher average neutron energy than the equivalent fission sources, with structure in the neutron energy spectrum due to the various transitions involved in the AmBe source reactions [3, 24–26]. The fission neutron spectra are distinct from that of the AmBe source and share similar distributions to each other, with the peak intensity at ~1 MeVee [21]. For general use as a neutron source, ^{252}Cf was highlighted as having an advantage over (α,n) sources due to its 'soft neutron spectra and low gamma activity' [27], although in the case of acting as a proxy for SNM, the reduced γ-ray emission may be considered a disadvantage.

A second key property of the fissile materials, that of the neutron multiplicity, is shown for key radionuclides in table 1. Clearly this is not a characteristic of an (α,n) source such as the AmBe, but for spontaneous fission of ^{240}Pu and ^{252}Cf (and to a lesser extent with its extremely low cross section, ^{239}Pu) there are more neutrons available per disintegration. Other techniques and algorithms focus on this property, separating based on the 'burstiness' of detected events [28] while PSD is not concerned with intra-event timing in its analysis beyond the avoidance of pulse pile-up for extremely high rates.

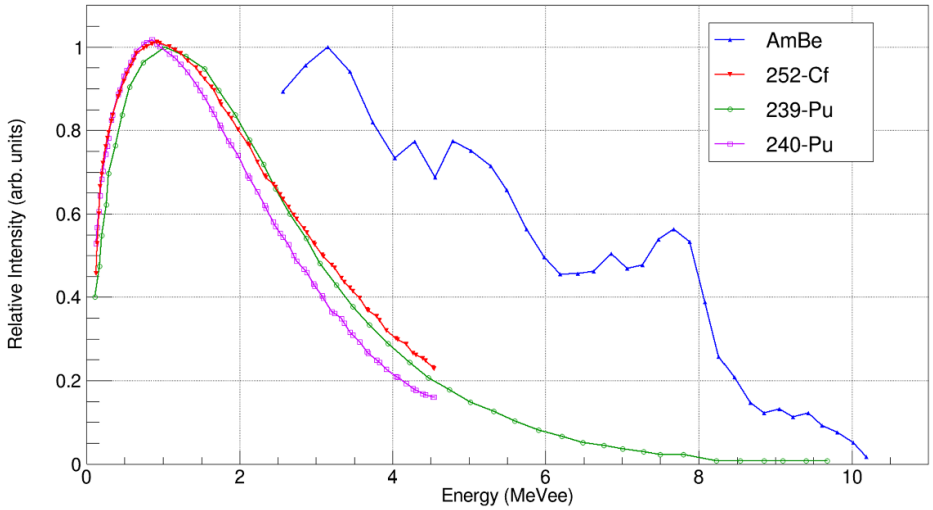

Figure 1. Example neutron spectra (normalised to their peak emission) reproduced from [3], [4], and [5]. Note the use of MeV electron equivalent here (and throughout) due to the light yield dependence on particle type and the respective quenching effects [6].

Table 1. Neutron yields and multiplicities (where applicable) for the sources and isotopes of interest [28, 35, 36].

Source	Mean multiplicity	Neutron yield ($s^{-1}g^{-1}$)
AmBe	–	1.3×10^{11}
^{239}Pu	2.16	3×10^{-2}
^{240}Pu	2.152	1×10^{3}
^{252}Cf	3.76	2.3×10^{12}

Detection of nuclear materials, such as uranium and plutonium, is rarely in the context of a clean signature performed in ideal laboratory conditions. The anticipated search location may well contain some level of moderation or shielding, whether intentional or otherwise. Therefore not only is it important to assess the performance of any detection system on SNM itself, but also using a variety of high-Z and hydrogenous shielding configurations in order to vary the γ and neutron flux incident on the detector respectively.

In this work we discuss PSD tests on plastic scintillator using three different radio-isotope sources; a fast neutron/gamma AmBe source, and two fission sources containing ^{252}Cf and special nuclear material (SNM). We also investigate the effectiveness of adding additional gamma sources in combination with the neutron sources to more closely replicate the spectra and detector neutron/gamma separation performance when in the presence of an SNM source.

2. Experimental setup

All measurements in this work used a detector consisting of PSD-sensitive scintillator directly coupled to SensL SiPMs. The detector was used to measure the energy response and neutron-gamma discrimination performance for each of the neutron sources studied.

Table 2. Prominent γ ray decay energies for ^{239}Pu [29, 30, 47]. The energy resolution of the plastic scintillator is generally insufficient to distinguish between peaks of these and their less intense satellite emissions.

Decay energy (keV)	Intensity (%)
111.298	1.33×10^{-3}
129.296	6.31×10^{-3}
375.054	1.554×10^{-3}
413.713	1.466×10^{-3}
451.481	1.894×10^{-4}
645.94	1.52×10^{-5}
658.86	9.70×10^{-6}
727.9	1.24×10^{-7}
756.4	2.8×10^{-6}
769.37	6.8×10^{-6}

As potential 'SNM proxy' sources we used AmBe and ^{252}Cf radionuclide sources. The AmBe source had an activity of ~18 GBq and was contained within a water tank of dimensions 80 cm $\times$ 76 cm $\times$ 94 cm. An air-tube was inserted to select fast neutrons, resulting in a source-detector offset of ~50 cm. Additionally, the standard configuration included 5 cm of lead shielding in order to reduce the γ-ray signal and achieve approximately a 50:50 n-γ ratio, full details can be found in earlier works [7, 8]. The ^{252}Cf source used in this study was mounted in air, offset from the detector due to the 5 cm lead shielding, and had an activity of 238 kBq.

Measurements were also taken using an enhanced AmBe source that consisted of an additional 118 kBq ^{133}Ba source placed in close proximity to the detector whilst setup as described previously. The addition of the ^{133}Ba signature, in particular the strong 356 keV γ ray gives a good approximation of the γ rays produced at low energies by ^{239}Pu, a (non-exhaustive) selection of prominent de-excitations are included as table 2.

The system was independently calibrated using laboratory γ ray sources at each measurement stage to ensure any potential drift in gain was accounted for. Due to the interaction of γ rays with plastic scintillators dominated by Compton scattering, it is not possible to resolve the primary photopeaks of commonly used sources (^{22}Na and ^{137}Cs) and so calibration is performed using the Compton edge of these γ rays, the full description is found in a previous publication [8]. Additionally, the current drawn by the SiPM was monitored throughout all experimental stages. To enable direct comparisons to be made between datasets measurements were taken with same level of shielding for the different sources such that the nature of the emitted radiation from each source was the only significant variable.

The performance of the detector was compared to measurements obtained using an SNM source consisting of 75 g of Pu with isotopic vectors consistent with those of low burn-up or weapons grade [31] plutonium (WGPu) at ~6% ^{240}Pu and ~93% ^{239}Pu. The majority of the neutron yield for plutonium sources is a result of the ^{240}Pu content [32], as shown in table 1 alongside yields for the other sources, whereas the γ signature is due to the presence of ^{239}Pu, its decay chain, and the ^{241}Am and ^{237}U daughters of ^{241}Pu [33, 34]. As well as the direct comparison of 5 cm of lead shielding further configurations of different thicknesses of both γ ray and neutron shielding as well as stand-off distances were investigated.

2.1. Silicon photomultiplier

The SensL J-series SiPM was selected for its very low dark current and excellent photon detection efficiency (PDE) in the emission range of interest. The performance of this SiPM had been previously tested and shown to give good n-γ separation with plastic scintillator [8]. The 6 mm J-series was used for all measurements, with two SiPM configurations used in this work. The MicroFJ-60 035-SMA is an evaluation board prepared by SensL housing a single 6 mm SiPM and was used with an appropriated sized scintillator described in the following section, these data are tagged as 'singles'. Additionally, a 2×2 array, the ArrayJ-60 035-4P-PCB, was mounted on bespoke read-out circuitry with all channels summed. Measurements with this detector are referred to as 'quads'.

2.2. Plastic scintillator

Two Eljen PSD sensitive plastic scintillators were investigated. The performance of the earlier formulation, EJ-299-34 [1, 7], was compared to the newer EJ-276 plastic scintillator [2, 8] which generally showed superior neutron-γ discrimination.

Each scintillator material was tested for cubes of 6 mm and 15 mm for use with the single and quad SiPM respectively. All faces were highly polished (0.3 μm), with one face optically coupled to the SiPM with Silicone High-Vacuum grease and the remaining faces either painted with EJ510 titanium oxide paint in the case of the EJ-299-34 scintillator, or wrapped in several layers of PTFE tape for the EJ-276 [37]. We have previously shown that there is negligible difference between the performance of the two reflective coatings when tested with identically prepared samples of EJ-299-34.

2.3. Data acquisition

Measurements were taken by acquiring waveform pulses in an event-by-event mode, using either a CAEN V1730C digitiser (AmBe data) or a CAEN DT5730B digitiser (fission source data). Both digitisers incorporated a 14-bit ADC operating over a dynamic range of 0.5 V_{pp} at a sample rate of 500 MHz. The CAEN digitisers utilise a multi-buffer technique in order to minimise deadtime effects [38]. However, for the unshielded SNM measurements the count-rate was sufficiently high that the detector was re-positioned further from the source to minimise deadtime.

The V1730C was connected via optical link cable to a CAEN A3818 optical controller in the acquisition PC, whereas the DT5730B was connected to its control computer with a standard USB cable.

2.4. Pulse shape discrimination

The PSD technique exploits the characteristic interaction mechanisms in order to identify the type of incident radiation. Full details of the phenomenon have been discussed in many previous works [39–41]; for scintillation light which contains emissions of different time constants *'the fraction of light that appears in the slow component often depends on the nature of the exciting particle'* [6]. Particles with higher linear energy transfer coefficients, such as neutrons in this case, produce scintillation with a greater proportion of the slow component, and thus can be distinguished from γ rays via a variety of algorithms.

In this study we used a charge comparison technique to determine a PSD parameter for each event [7, 8], which uses the ratio of the integrated charge in the prompt portion of the pulse to

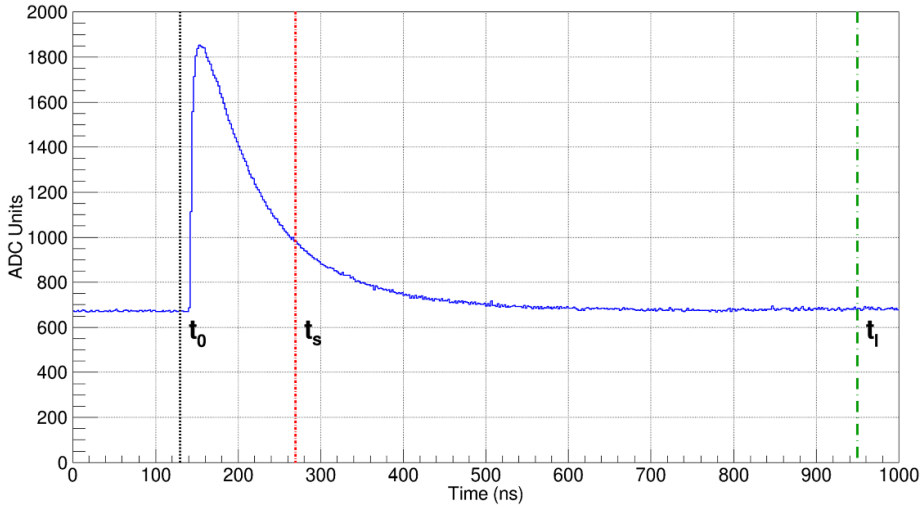

Figure 2. The charge comparison method. Each pulse is processed in the same way, whereby the charge, Q_s, in a defined 'short' time window from t_0 to t_s, is compared to that of the whole pulse, where Q_l is the charge integrated from t_0 to t_l. Note how the regions of Q_s and Q_l overlap for this algorithm.

the total integrated charge. The value of this ratio is different for incident neutrons compared to γ rays due to the respective interaction mechanisms of each species [41, 42]. This is shown graphically in figure 2 and described by:

$$Q_s = \int_{t_0}^{t_s} y(t)\,\mathrm{d}x \tag{1}$$

$$Q_l = \int_{t_0}^{t_l} y(t)\,\mathrm{d}x \tag{2}$$

where t_0 is the start time of the two gates, t_s the end time of the short gate, and t_l the end time of the long gate.

The PSD parameter is then determined by a ratio of these components:

$$PSD = 1 - \frac{Q_s}{Q_l}. \tag{3}$$

Additionally, the quantity Q_l, the long gate charge, is proportional to the energy of the event, which, when plotted against the PSD parameter forms a distinctive forked histogram (see later figure 3) from which the degree of neutron-γ separation can be determined. A projection of the PSD parameter shows a double Gaussian distribution, and the degree of neutron-γ separation is described by a figure of Merit (FoM) parameter [43] defined as:

$$FoM = \frac{S}{\Gamma_n + \Gamma_\gamma}, \tag{4}$$

where S is the centroid separation, Γ_n is the FWHM of the neutron peak, and Γ_γ the γ FWHM.

Table 3. Selected figures of Merit for the reported scintillator-photodetector combinations (6 mm data previously published in [8]) highlighting the performance increase of the new scintillator as well as the reduction in FoM for larger sizes.

		FoM		
Detector	Scintillator	500 keVee	1 MeVee	1.5 MeVee
Single	EJ-299	1.72 ± 0.01	2.02 ± 0.02	2.12 ± 0.03
	EJ-276	2.39 ± 0.01	2.84 ± 0.02	3.03 ± 0.03
Quad	EJ-299	1.17 ± 0.01	1.42 ± 0.01	1.51 ± 0.01
	EJ-276	2.21 ± 0.01	2.25 ± 0.02	2.18 ± 0.03

3. Results and discussion

We describe the PSD performance of the scintillator in the presence of neutron-γ mixed radiation fields from the various sources, with the γ and neutron spectra shown independently. The detectors' tolerance to various shielding configurations and the impact of shielding upon the neutron-γ ratio will be assessed. The effectiveness of the various radionuclide sources in acting as SNM proxy sources will be described.

3.1. PSD performance

Using the charge comparison technique the PSD parameter for each event is plotted against the total energy of the pulse as shown in figure 3 for the mixed radiation fields of each source as well as for a γ-only source of ^{22}Na to provide a comparison. For this algorithm, a mixed radiation field exhibits two loci, where the upper locus contains the neutron events whereas the lower locus contains the γ ray events. It can be seen that γ only events from a ^{22}Na source aligns with the lower locus of the other plots. The data displayed in figure 3 were obtained using the 15 mm cube of EJ-276 with the 'standard' 5 cm lead shielding configuration.

The degree of neutron-γ separation is calculated from the PSD spectrum (a Y-axis projection of the 2D histogram), for various energy thresholds. Full details of our use of the figure of merit (FoM) calculation as defined by [43] are given in [7, 8]. As an example the projection of the AmBe PSD parameter and its double peak form, is shown in figure 4 with 100 keV$_{ee}$ energy threshold bands applied. It is clear that while the centroid of the γ peak remains relatively constant the neutron peak has a noticeable shift in centroid position.

Table 3 shows the measured PSD performance obtained for Eljen EJ-299-34 and EJ-276 scintillators when irradiated with a mixed fast neutron/gamma field from the AmBe source, using 'single' 6 mm and 'quad' 15 mm scintillator cubes. Good PSD performance is generally defined as a 3σ separation of the neutron and γ peaks [1, 44], which equates to a FoM of 1.27. The 15 mm cube generally provides poorer PSD performance than the smaller scintillator, which fits the commonly observed trend in these plastic scintillators of worsening PSD performance as the volume of the scintillator increases [45, 46]. It can be seen from table 3 that for the EJ-299 material the PSD performance at a threshold of 500 keV$_{ee}$ fails to meet the 3σ criterion. In contrast, the PSD performance for the EJ-276 scintillator significantly exceed the 3σ criterion at all measured energy values. When considering the 'improvement' ratio of the FoM values between EJ-276 and EJ-299, for the small detectors the improvement is a constant factor of 1.4 for all three energy values. For the large detector the improvement in performance of EJ-276 compared to EJ-299 is even more noticeable, with a ratio of 1.9 at 500 keV$_{ee}$, reducing to 1.4 at 1.5 MeV$_{ee}$.

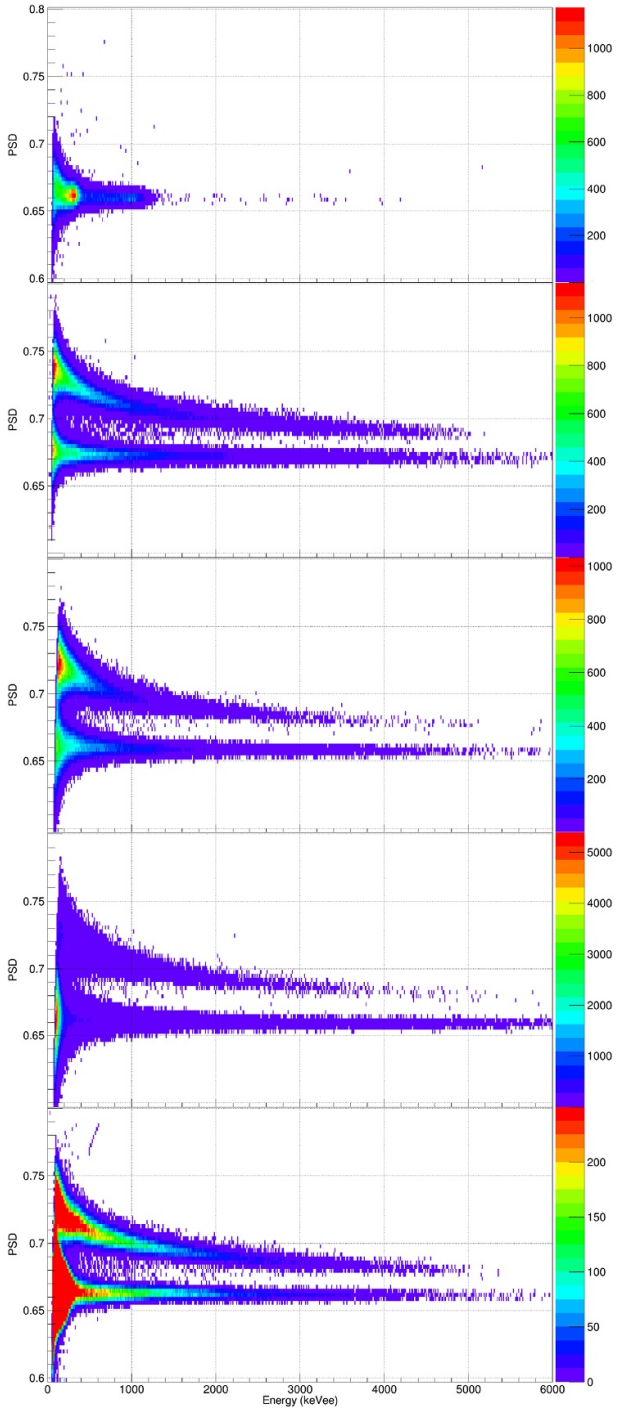

Figure 3. The PSD Vs Energy plots acquired from the 15 mm EJ-276 detector. From top to bottom: reference ^{22}Na, AmBe, ^{252}Cf, SNM, and enhanced AmBe (the *Z*-axis range for the enhanced AmBe has been adjusted to allow the PSD structure to be visible.

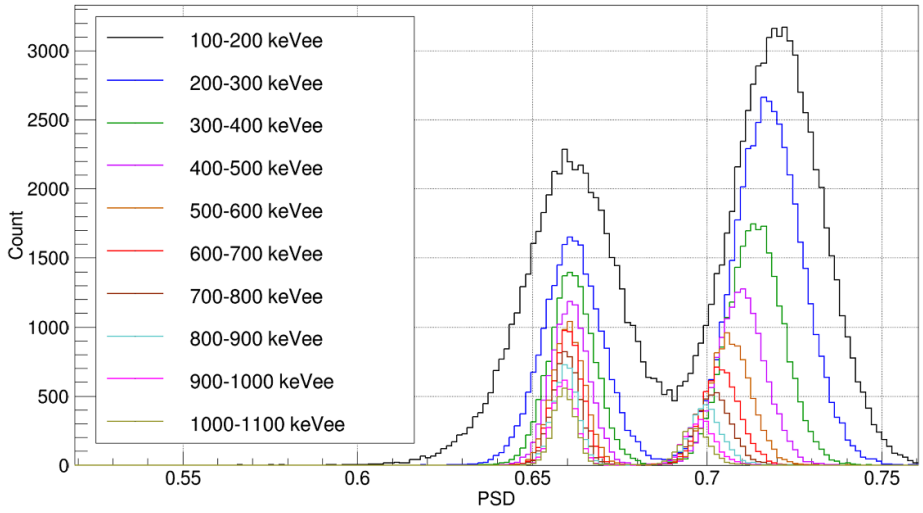

Figure 4. The PSD projections for AmBe source data after the application of 100 keV$_{ee}$ energy gates.

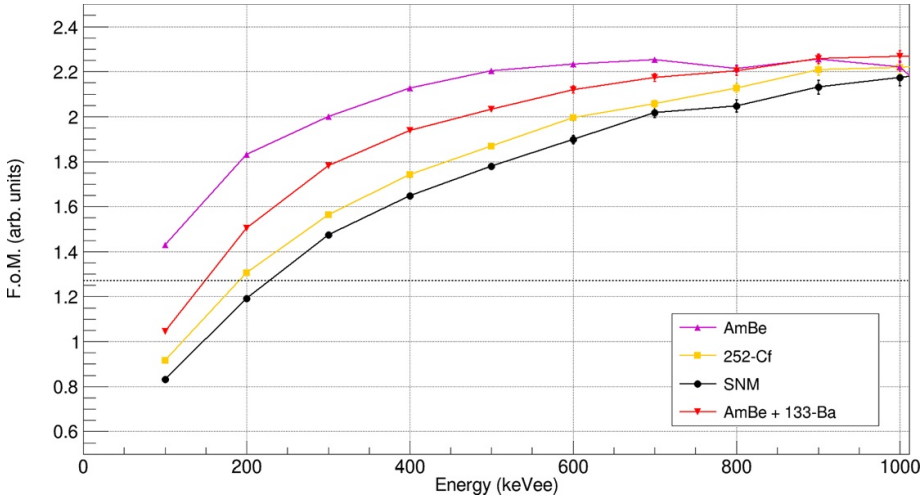

Figure 5. The lower energy (0–1 MeV$_{ee}$) FoM for the data displayed in figure 3. The dashed line corresponds to the FoM = 1.27 threshold.

Figure 5 shows the FoM values obtained from the 15 mm EJ-276 detector for each source, as a function of energy up to 1 MeV$_{ee}$. In general the same trend of increasing FoM as a function of increasing energy is observed across all four sources. The measured FoM from ^{252}Cf closely approximates the separation achieved for SNM over the full energy. In contrast, for energies below ~800 keV$_{ee}$ the FoM values obtained from the AmBe mixed radiation field are significantly higher than for the other sources. However, once the ~1 MeV$_{ee}$ threshold is reached, the four sets of FoM values become comparable. This convergence of source FoM is also shown in table 4 highlighting some key FoM values for the 'quad' detector with each

Table 4. Selected 'low energy' figures of Merit for the EJ-276 Quad detector in the mixed radiation fields of different sources.

	FoM		
Source	100 keVee	250 keVee	500 keVee
AmBe	1.44 ± 0.01	1.97 ± 0.01	2.21 ± 0.01
^{252}Cf	0.92 ± 0.01	1.46 ± 0.01	1.87 ± 0.01
SNM	0.82 ± 0.01	1.35 ± 0.01	1.78 ± 0.01

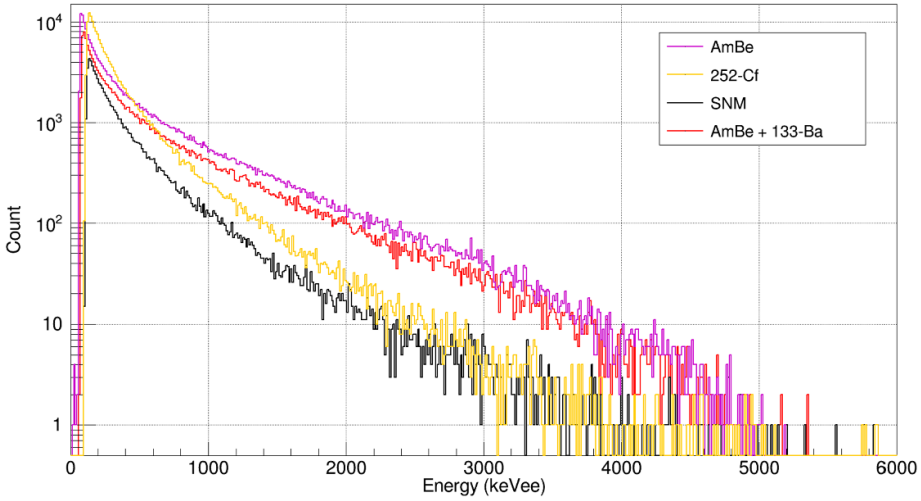

Figure 6. The extracted neutron spectra.

source. At 100 keVee the required level of separation is only achieved in AmBe source's radiation field, indicating an over-estimate of separation when used as a proxy at these energies. However, the difference between the degree of n-γ discrimination for an (α,n) source and a fission source reduces at 500 keVee, and is further reduced by the 1 MeVee threshold.

To explain the variation in measured FoM between the different sources (shown in figure 5 and table 4) it is necessary to examine the neutron and γ ray spectra in each case. These have been extracted from each of the 2D histograms and are displayed in figures 6 (neutron) and 7 (γ ray). Due to the nature of the proton recoil mechanism that is used to detect fast neutrons, the raw deposited energy spectrum from plastic scintillators do not directly reflect the incident neutron energy spectrum. For this reason, the measured neutron spectrum from the AmBe source shown in figure 6 does not show the structure that is visible in figure 1. However, the measured neutron energy spectrum does show a distribution of higher energy neutrons in the AmBe spectrum which is not present in the fission sources which follow the Watt distribution [20].

From the γ spectra shown in figure 7 it is clear that the most significant difference in spectral shape between the sources is the different intensities of γ rays at energies below approximately 400 keV. The SNM source shows a large contribution of low energy γ rays which is primarily a result of the decay chain products of ^{239}Pu [33, 34]. This feature explains the reduction in FoM, as displayed in table 4 and figure 5, for the SNM sample compared to that of the ^{252}Cf source at the lower energy thresholds, and the subsequent improvement in FoM of the SNM

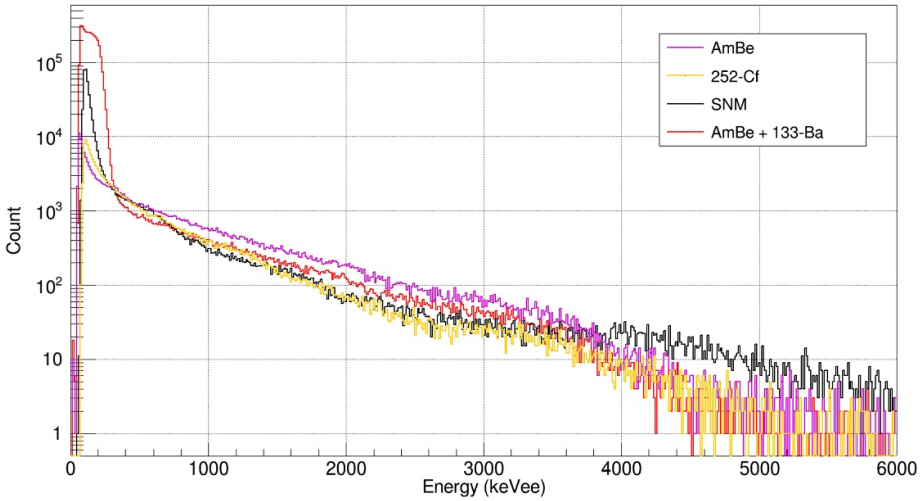

Figure 7. The extracted γ spectra.

Table 5. Shielding configurations investigated throughout this work. The pictogram shows an image approximating the experimental setup, where the green star represents the neutron source, grey and blue boxes show where lead or HDPE was used respectively, and the detector position is given by the red trapezium. For the enhanced AmBe/^{133}Ba measurement, the ^{133}Ba source was placed adjacent to the detector and not shielded.

Pictogram	Source	Description	Duration	FoM(500 keV$_{ee}$)
	AmBe	5 cm lead	20 h	2.21 ± 0.01
	AmBe/^{133}Ba	5 cm lead	20 h	2.03 ± 0.01
	^{252}Cf	5 cm lead	20 h	1.87 ± 0.01
	SNM	5 cm lead	20 h	1.78 ± 0.01
		Unshielded (5 cm)	2 h	~1.9
		Unshielded (10 cm)	13 m	–
		10 cm lead	20 h	1.83 ± 0.01
		10.6 mm lead at 10 cm	1 h	–
		5 cm lead & 5 cm HDPE	20 h	1.75 ± 0.04
		10 cm HDPE at 15 cm	1 h	–

source as energy increases. Similarly, the mixed AmBe and ^{133}Ba source shows a significantly higher intensity of low energy γ rays, e.g. due to the presence of 356 keV γ rays from ^{133}Ba and a resulting reduction in the FoM at low energies.

3.2. Detection of SNM

Further studies were made of the detectors' performance with the AmBe and ^{252}Cf sources using a variety of shielding configurations in addition to the 'standard' arrangement described previously (5 cm lead). These configurations are listed in table 5 along with a pictogram demonstrating the setup. Due to time constraints of the measurements, the counting durations were not constant for each configuration, with times ranging from ~10 min to overnight

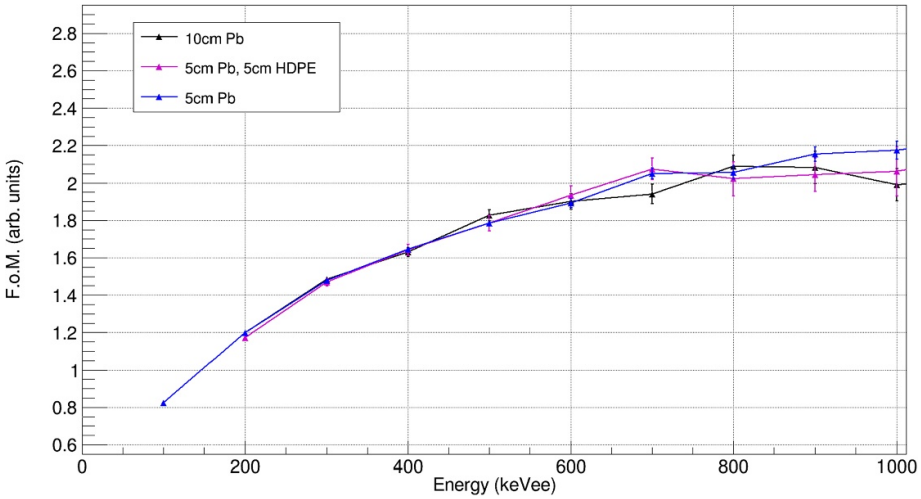

Figure 8. The low-energy FoM for different shielding configurations. Below 200 keV$_{ee}$ it was not possible to achieve a good FoM fit for the '10 cm Pb' and '5 cm Pb and 5 cm HDPE' datasets.

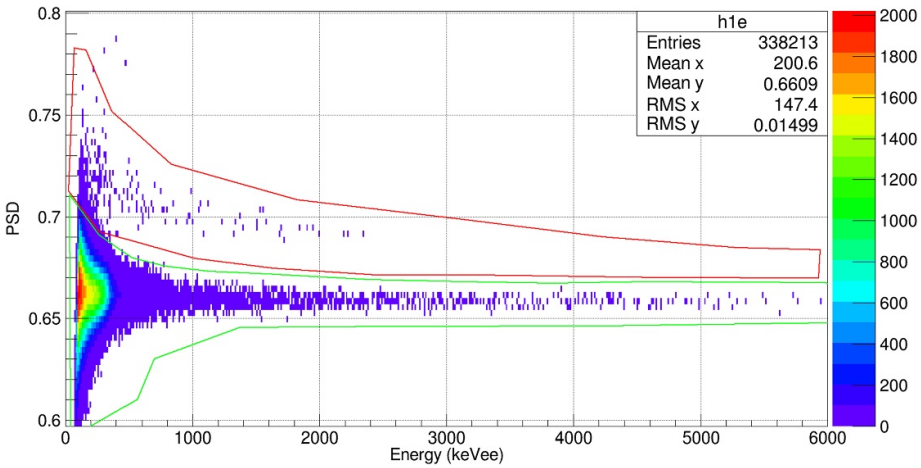

Figure 9. The PSD V Energy histogram for 10 cm HDPE neutron shielding of the SNM source. The red and green gates were determined using the 'standard' shielding configuration data (5 cm Pb), with red the likely neutron events, and green surrounding likely γ-ray pulses.

runs of ~20 h. The shortest runs were those dominated by the significant γ flux of unshielded measurements where data rates were highest.

The longest duration measurements were the three configurations: (i) 5 cm lead, (ii) 10 cm lead, and (iii) 5 cm lead plus 5 cm HDPE, which enabled the full PSD analysis to be performed. These results are shown in figure 8. These data show a consistent trend in FoM for the three shielding configurations, although at energies above about 1 MeV$_{ee}$ the reduction in statistics increases the error bars that are derived from the double Gaussian fit. This is particularly pronounced for the 10 cm Pb shielding dataset where the number of neutron events at high energy drops to ~10 per bin.

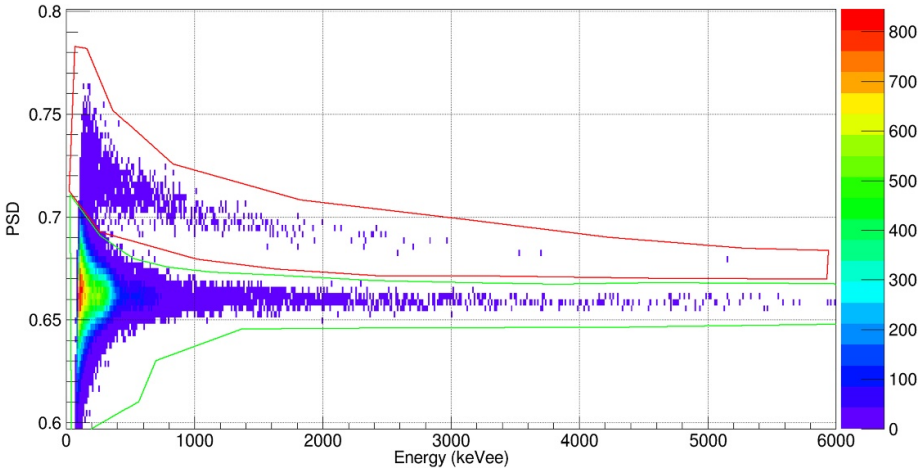

Figure 10. The PSD V Energy histogram for 1 cm Pb shielding of the SNM source. The red and green gates were determined using the 'standard' shielding configuration data (5 cm Pb), with red the likely neutron events, and green surrounding likely γ-ray pulses.

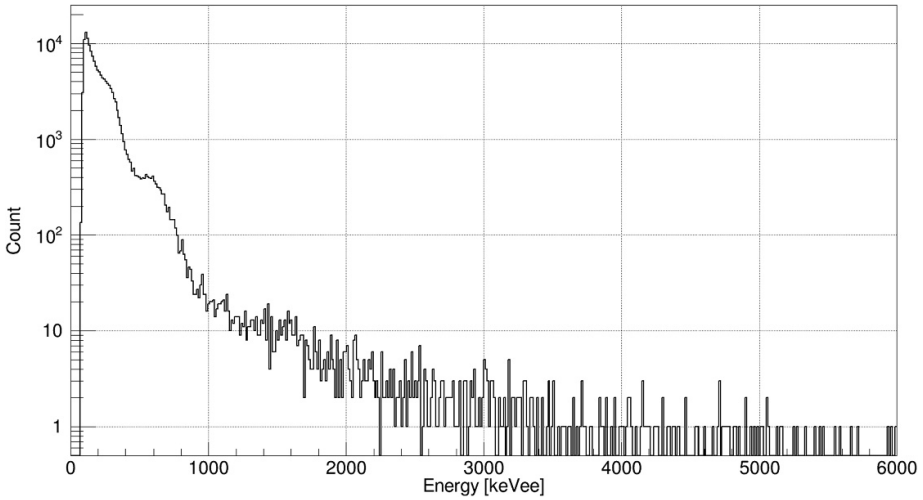

Figure 11. The γ-ray spectra from the 1 cm Pb shielding SNM source dataset shown in figure 10.

The datasets for the remaining configurations were dominated by the significant γ-ray flux incident on the detector. As a result, for many of these configurations, it was not possible to achieve statistically meaningful FoM, particularly at higher energy thresholds. However, in all of these cases events were identified within the neutron locus established with the standard shielding configuration that were cleanly separated from the PSD γ-ray peak. This is shown in figures 9 and 10, both configurations with 'short' durations of ~1 h.

Figure 10 was acquired using an SNM source with Pb shielding of only 1 cm thickness. Compared to 5 cm of Pb shielding, this configuration only weakly attenuated the γ rays and the γ spectrum of the source becomes apparent as shown in figure 10. There are features at ~350 and 730 keV_{ee} which corresponds broadly to the Compton edges of known energies for

WGPu γ lines [33, 47]. However, it is the nature of plastic scintillators that such an assessment will always be an approximation.

4. Conclusion

We have shown in this work the functionality of a compact neutron-γ discriminating detector for use in detecting SNM. The relative response to a number of different neutron sources has been investigated and the degree of neutron/γ discrimination with respect to energy has been determined. We conclude that depending on the intended purpose ^{252}Cf and AmBe are efficient proxies when an SNM source is unavailable. However, care must be taken to consider the energy range of interest, with AmBe sources providing a more intense distribution of higher energy neutrons compared to SNM. In terms of γ emission, the low-energy γ rays emitted from SNM are under represented by AmBe and fission sources and these proxies will typically over-estimate the FoM performance of a system intended to detect SNM. To mitigate this issue a more realistic signature can be made using the addition of another radionuclide to the neutron source. The chosen enhancement depends somewhat on the target material, with ^{57}Co often used where highly enriched uranium (HEU) is of concern [48], but for ^{239}Pu this role is performed by ^{133}Ba [49], and this work has demonstrated that similar FoM results can be obtained from such a combination proxy source. The introduction of the ^{133}Ba into the spectrum has the effect of reducing the n-γ ratio from that of pure AmBe, to a closer approximation of SNM (in our case the respective activities more closely aligned to the dual shielded 5 cm Pb/HDPE measurement). However, this adjustment is no longer apparent after ~400 keV$_{ee}$, a combination of the 356 keV γ ray and the harder neutron spectra of AmBe in comparison to that of ^{239}Pu. Further enhancement could be provided by considering narrower energy regimes, and providing a proxy source at each point. This has been tested by other groups [48, 49], although with the plastic scintillator tested here, the low resolution prevents spectroscopic information being discernable. The further addition of ^{241}Am, ^{109}Cd, and ^{137}Cs was shown to provide a good replication of plutonium spectra [49]. Conversely, here we have looked at the variation in detector response where a real SNM source is shielded, approaching the problem from the opposite direction.

With the successful performance of this system in mind, the next stages of development must surely be in the direction of deployable equipment. Current radiation portal monitors use substantially larger volumes of scintillator than have been investigated in this work, and it has been shown previously that scintillator size has a direct effect on PSD performance [45, 46]. The degradation observed in PSD as detector volume increases is a combination of parameters: the optical attenuation as the photon transverses the scintillator; the increased variation in transit time due to multiple reflections within the material; and the relatively similar durations of neutron and γ ray time constants. The increased attenuation results in smaller pulses and therefore less light/charge available for collection, which, in analogy to a low energy interacting particle, can be seen from figure 3 makes separation more difficult. The variation in transit time, coupled with the respective time constants [8], effectively smears out the average pulse shapes, resulting in less defined, and therefore less separable neutron- and γ-ray indicative signals. Ongoing parallel research threads are investigating larger scale PSD systems [50].

Similarly, this work made use of traditional crate-based data acquisition (DAQ) systems, which clearly are unsuitable for any field role. To be able to deploy a detector such as that showcased here it will be necessary for a compact DAQ to be developed alongside the front-end scintillator-photodetector system.

ORCID iDs

Matthew P Taggart https://orcid.org/0000-0003-4282-3227
Michael W J Hubbard https://orcid.org/0000-0002-4378-826X
Paul J Sellin https://orcid.org/0000-0002-5221-0515

References

[1] Zaitseva N P *et al* 2012 Plastic scintillators with efficient neutron/gamma pulse shape discrimination *Nucl. Instr. Meth.* A **668** 88–93
[2] Zaitseva N P *et al* 2018 Recent developments in plastic scintillators with pulse shape discrimination *Nucl. Instr. Meth.* A **889** 97–104
[3] Lorch E A 1973 Neutron spectra of ^{241}Am/B, ^{241}Am/Be, ^{241}Am/F, ^{242}Cm/Be, ^{238}Pu/^{13}C and ^{252}Cf isotopic neutron sources *Int. J. Appl. Radiat. Isot.* **24** 585–91
[4] Ohsawa T, Horiguchi T and Mitsuhashi M 2000 Multimodal analysis of prompt neutron spectra for ^{238}Pu(sf), ^{240}Pu(sf), ^{242}Pu(sf) and ^{239}Pu(n_{th},f) *Nucl. Phys.* A **665** 3–12
[5] Craig R A and Bliss M 2000 Predicted Performance of Neutron Spectrometers Using Scintillating Fibers *Technical Report* Pacific Northwest National Laboratory **PNNL-13111**
[6] Knoll G F 2000 *Radiation Detection and Measurement* (New York: Wiley)
[7] Taggart M P *et al* 2016 Neutron-gamma discrimination via PSD plastic scintillator and SiPMs *J. Phys. Conf. Series* **763** 012007
[8] Taggart M P *et al* 2018 Comparison of the pulse shape discrimination performance of plastic scintillators coupled to a SiPM *Nucl. Instr. Meth.* A **908** 148–54
[9] Buffler A, Corrie A C, Smit F D and Wörtche H J 2016 A new compact neutron/gamma ray scintillation detector *Int. J. Nucl. Tech.* **44** 1660228
[10] Blanc P *et al* 2014 Neutron/gamma pulse shape discrimination in plastic scintillators: preparation and characterization of various compositions *Nucl. Instr. Meth.* A **750** 1–11
[11] D'Mellow B *et al* 2007 Digital discrimination of neutrons and γ-rays in liquid scintillators using pulse gradient analysis *Nucl. Instr. Meth.* A **578** 191–7
[12] Flaska M and Pozzi S A 2007 Identification of shielded neutron sources with the liquid scintillator BC-501A using a digital pulse shape discrimination method *Nucl. Instr. Meth.* A **577** 654–63
[13] Liao C and Yang H 2015 Pulse shape discrimination using EJ-299-33 plastic scintillator coupled with a Silicon Photomultiplier array *Nucl. Instr. Meth.* A **789** 150–7
[14] Hamel M *et al* 2014 A flurocarbon plastic scintillator for neutron detection: Proof of concept *Nucl. Instr. Meth.* A **768** 26–31
[15] Ellis M *et al* 2017 Neutron and gamma ray pulse shape discrimination with EJ-270 lithium-loaded plastic scintillator *IEEE Nuclear Symp. Conf. Record* pp 1–5
[16] Balmer M J I, Gamage K A A and Taylor G C 2015 Comparative analysis of pulse shape discrimination methods in a ^{6}Li-loaded plastic scintillator *Nucl. Instr. Meth.* A **788** 146–53
[17] Cieslak M J, Gamage K A A and Glover R 2017 Pulse shape discrimination characteristics of stilbene crystal, pure and ^{6}Li-loaded plastic scintillators for a high resolution coded-aperture neutron imager *JINST* **12** P07023
[18] Lovins A B 1980 Nuclear weapons and power-reactor plutonium *Nature* **283** 817–23
[19] Mark J C 1993 Explosive Properties of reactor – grade plutonium *Sci. Global Security* **4** 111–28
[20] Watt B E 1952 Energy spectrum of neutrons from thermal fission of U235 *Phys. Rev.* **87** 1037–42
[21] Smith A B, Fields P R and Roberts J H 1957 Spontaneous fission neutron spectrum of Cf252 *Phys. Rev.* **108** 411–13
[22] Sugimoto M, Smith A B and Guenther P T 1987 Ratio of the prompt fission neutron spectra of ^{239}Pu to that of ^{235}U *Nucl. Sci. Eng.* **97** 235–8
[23] Hess W N 1959 Neutrons from (α,n) Sources *Ann. Phys. NY* **2** 115–33
[24] Thompson M N and Taylor J M 1965 Neutron spectra from Am-α-Be and Ra-α-Be sources *Nucl. Instr. Meth.* **37** 305–8
[25] Coelho P R P, Silva A A D and Maiorino J R 1989 Neutron energy spectrum measurements of neutron sources with an NE-213 spectrometer *Nucl. Instr. Meth.* A **280** 270–2
[26] Geiger K W and Zwan L V D 1970 The neutron spectrum of a ^{241}AmBe(α,n) source as simulated by accelerator produced α particles *Int. J. Appl. Radiat. Isotopes* **21** 193

[27] Karenlin Y A *et al* 1997 Californium-252 neutron sources *Appl. Radiat. Isot.* **48** 1563–6
[28] Ensslin N *et al* 1998 Application guide to neutron multiplicity counting *Technical Report* LA-13422-M
[29] Gunnink R and Morrow R J 1971 Gamma-ray energies and absolute branching intensities for ^{238,239,240,241}Pu and ^{241}Am *Technical Report* UCRL-51087
[30] Sampson T E 1986 Plutonium isotopic composition by gamma-ray spectroscopy: a review *Technical Report* LA-10750-MS
[31] Morrison S L, Lindley B A and Parks G T 2018 Isotopic and spectral effects of Pu quality in Th-Pu fueled PWRs *Ann. Nucl. Energy* **117** 318–32
[32] DoE U *Nonproliferation and arms control assessment of weapons-usable fissile material storage and excess plutonium disposition alternatives* (DOE/NN-0007) doi: 10.2172/425259
[33] Gosnell T B and Wong J L 2014 Rapid, autonomous analysis of HPGe gammaray spectra III: Plutonium identification and characterization *Technical Report* Lawrence Livermore National Laboratory LLNL-TR-650534
[34] Gunnink R, Evans J and Prindle A 1976 A re-evaluation of the gamma-ray energies and absolute branching intensities of 237U, 238,239,240,241Pu and 241Am *Technical Report* Lawrence Livermore Laboratory UCRL-52139
[35] Passive Nondestructive Assay of Nuclear Materials 2007
[36] Lestone J P 2014 Energy and isotope dependence of neutron multiplicity distributions *Technical Report* Los Alamos National Laboratory LA-UR-05-0288
[37] SensL, Wrapping scintillator crystals to optimize light collection *Technical Report Sense Light* (www.sensl.com/downloads/ds/TN-Crystal_wrapping.pdf)
[38] CAEN, Gudie GD2080 - Introduction to Digitizers, (February 2014) (www.caen.it/csite/CaenProd.jsp?idmod=780&parent=11#)
[39] Birks J B 1964 *The Theory and Practice of Scintillation Counting* (Oxford: Pergamon)
[40] Brooks F D 1979 Development of organic scintillators *Nucl. Instr. Meth.* **162** 477–505
[41] Ranucci G 1995 An analytical approach to the evaluation of the pulse shape discrimination properties of scintillators *Nucl. Instr. Meth.* A **354** 389–99
[42] Brooks F D 1959 A scintillation counter with neutron and gamma-ray discriminators *Nucl. Instr. Meth.* **4** 151–63
[43] Winyard R A, Lutkin J E and McBeth G W 1971 Pulse shape discrimination in inorganic and organic scintillators I *Nucl. Instr. Meth.* **95** 141–53
[44] Lintereur A, Ely J, Stave J and McDonald B 2012 Neutron and gamma ray pulse shape discrimination with polyvinyltoluene *PNNL Technical Report* **21609**
[45] Ellis M *et al* 2013 The effect of detector geometry on EJ-309 pulse shape discrimination performance *IEEE Nuclear Symp. Conf. Record* pp 1–6
[46] Kendall P A *et al* 2014 Comparative study of the pulse shape discrimination (PSD) performance of fast neutron detectors *IEEE Nuclear Symp. Conf. Record* pp 1–6
[47] NuDat 2.7 2018 https://www.nndc.bnl.gov (Accessed October 2018)
[48] Scholz Z, Millett M and Schell M 2018 Evaluation of highly enriched uranium (HEU) surrogate sources for use in training and modeling *Nucl. Instr. Meth.* A **910** 139–46
[49] Peerani P and Tomanin A 2011 Surrogates of plutonium for detection equipment testing *Nucl. Instr. Meth.* A **654** 613–20
[50] Hubbard M W J 2020 Unpublished *PhD Thesis* University of Surrey